Engineering Turbulence Modelling and Experiments – 5
W. Rodi and N. Fueyo (Editors)

PREDICTION OF TURBULENT HEAT TRANSFER IN STATIONARY AND ROTATING U-DUCTS WITH RIB ROUGHENED WALLS

Jonas Bredberg[1] [2] and Lars Davidson

Chalmers University of Technology,
Department of Thermo and Fluid Dynamics,
SE-412 96 Gothenburg, Sweden

ABSTRACT

Numerical simulations of a stationary and rotating rib-roughened U-bend at high Reynolds number, $Re_D = 95\,000$, are presented. Using a recently developed $k-\omega$ turbulence model, the predicted velocity and heat transfer in the two legs of the U-bend are in excellent agreement with measured data. In the bend, the streamline curvature makes any unmodified eddy-viscosity models inadequate and hence larger discrepancies are found. Similarly to the measurements the model predicts increased heat transfer downstream the bend, due to the higher levels of turbulence. Under rotating conditions, $Ro = 0.2$, the model faithfully alters the predicted Nusselt number, to as high as 30% above those for the non-rotating case. To reduce computational demands a newly developed wall treatment is applied to the baseline model, enabling a relatively coarse mesh, with a first interior node location at $y^+ \approx 5$, to be used. The wall treatment which is based on the near-wall variation of flow variables, reduces the mesh dependency, and improves numerical stability.

1 INTRODUCTION

The efficiency and power output of gas-turbines are strongly connected to the operating gas-temperatures. For turbine blades working at extreme conditions, it is necessary to construct elaborate cooling systems which uses a large amount of cooling air. The cooling passages inside

[1]E-mail: bredberg@tfd.chalmers.se
[2]Present address: Volvo Aero Corporation, Military Engines Division, SE-461 81 Trollhättan

these blades involves serpentine ducts, with heat transfer enhancing devices, e.g. ribs. These ribs or turbulators when arranged orthogonally to the flow, will increase turbulence and hence the heat transfer level. In order to optimise the cooling process, it is most valuable to have accurate and detailed information of the flow-field and temperature levels in these cooling ducts. In this work predictions of heat and fluid flow in rotating and stationary rib-roughened 3D U-ducts in condition similar to those found in operating gas-turbines are performed.

It is well known that the prediction of heat transfer is highly sensitive to the location of the near-wall node. In the case of a $k-\omega$ turbulence model, the recommended number of nodes in the viscous sub-layer is seven to ten (Wilcox, 1993b), which puts great demands on mesh refinement. Using a turbulence model with wall functions, the mesh requirement is relaxed, however with a general deterioration of the predicted results. Employing wall-functions the near-wall variation of flow quantities are neglected, and its success is hinged on the universality of the wall-functions, which has been severely questioned (Launder, 1984).

Due to the limitations of the wall function approach and the necessities to reduce computational demands for the present geometry, a new methodology is needed. Similar difficulties have been experience by other groups, which have resulted in a number of approaches for improving coarse mesh predictions, e.g. Grotjans and Menter (1998), Bredberg et al. (2000), Craft et al. (2001), and Bredberg and Davidson (2002). In this paper the method presented in Bredberg and Davidson (2002) is adopted in conjunction with the recently developed $k-\omega$ turbulence model, Bredberg et al. (2002). The model is applied to a rib-roughened U-bend under both stationary and rotating conditions.

2 MODEL FORMULATION

The governing equations for an incompressible flow are the continuity equation, the momentum equations and the temperature equation. Applying the Reynolds averaging procedure results in an unclosed equation system. The unknowns, the Reynolds stress tensor, $\overline{u_i u_j}$, in the momentum equations and the heat flux vector, $\overline{u_i \theta}$, in the temperature equation, are modelled using the Boussinesq hypothesis and the standard gradient diffusion hypothesis respectively. In the model for the heat flux vector a constant turbulent Prandtl number is employed, with a value of, $Pr_t = 0.9$. The turbulent viscosity in the relation for the Reynolds stress tensor is here modelled using the $k-\omega$ turbulence model of Bredberg et al. (2002):

$$\nu_t = C_\mu f_\mu \frac{k}{\omega}, \qquad f_\mu = 0.09 + \left(0.91 + \frac{1}{R_t^3}\right)\left[1 - \exp\left\{-\left(\frac{R_t}{25}\right)^{2.75}\right\}\right] \tag{1}$$

$$\frac{Dk}{Dt} = P_k - C_k k\omega + \frac{\partial}{\partial x_j}\left[\left(\nu + \frac{\nu_t}{\sigma_k}\right)\frac{\partial k}{\partial x_j}\right] \tag{2}$$

$$\frac{D\omega}{Dt} = C_{\omega 1}\frac{\omega}{k}P_k - C_{\omega 2}\omega^2 + C_\omega\left(\frac{\nu}{k} + \frac{\nu_t}{k}\right)\frac{\partial k}{\partial x_j}\frac{\partial \omega}{\partial x_j} + \frac{\partial}{\partial x_j}\left[\left(\nu + \frac{\nu_t}{\sigma_\omega}\right)\frac{\partial \omega}{\partial x_j}\right] \tag{3}$$

R_t is the turbulent Reynolds number defined as $R_t = k/(\omega\nu)$. The constants in the model are given as

$$C_k = 0.09, \quad C_\mu = 1, \quad C_\omega = 1.1, \quad C_{\omega 1} = 0.49, \quad C_{\omega 2} = 0.072, \quad \sigma_k = 1, \quad \sigma_\omega = 1.8$$

Using this model improved results, compared to the low-Reynolds number $k-\omega$ model of Wilcox (1993a) were achieved for several flows, including rib-roughened channels. In many flows of engi-

neering interest, such as the rib-roughened U-bend, it is howver computationally too demanding to achieve a mesh refinement on a level required by a low-Reynolds number turbulence model.

To relax numerical resources, without using inadequate wall-functions, a new near-wall treatment (Bredberg and Davidson, 2002) is employed here. The method is based on asymptotic behaviour of flow quantities when approaching the wall, and applies corrections to compensate for numerical approximation made on coarse meshes. Modifications to the baseline model are made to the production term in the k-equation and the wall boundary condition for ω, respectively:

$$P_{k,mod} = \frac{2P_{k,std}}{1+0.9R_t} \tag{4}$$

$$\omega_w = f\omega_{LRN} + (1-f)\omega_{WF} \tag{5}$$

where ω_{LRN} is the asymptotic solution to the ω-equation (Eqn. 3), and ω_{WF} is the appropriate wall value for a logarithmic approach (Wilcox, 1993b). The smoothing function, f, is numerical optimised to $f = \exp(-y^*/17)$, where $y^* = u_\varepsilon y/\nu$ is the non-dimensional wall distance, using the Kolmogorov velocity scale. Note that these modifications are only applicable to the first interior node.

In the present contribution, coarse mesh numerical stability was further enhanced through incorporation of limiters for the cross-diffusion terms in the ω-equation:

$$CD = \min(CD^v, 0) + \min(fCD^T, 0) + \max(CD^T, 0), \qquad f = \exp\left[CD^T\nu_t/(C_k k\omega)\right] \tag{6}$$

where CD^v and CD^T are the viscous and turbulent cross-diffusion term respectively in Eqn. 3.

3 SOLUTION PROCEDURE

The model was implemented in the incompressible finite volume code CALC-BFC (Davidson and Farhanieh (1995)). The code employs the van Leer 2:nd order bounded differencing scheme for the convective derivates, and the 2:nd order central differencing scheme for the other terms. The SIMPLE-C algorithm is used to deal with the velocity-pressure coupling.

All variables were prescribed in the inlet, while the Neumann condition was used at the outlet. The results from a channel flow simulation provided a realistic variation across the channel in the inlet. On the walls, no-slip condition was used, $U_i = 0, k = 0$, with the boundary condition for ω is set using relation (5). A constant heat transfer rate was applied along the outer and inner walls.

In the experiment fine wire meshes and a honeycomb is included upstream the U-bend to ensure a symmetric and uniform flow in the measuring section. These flow controllers increase the level of turbulence, which need to be simulated in the computations. The exact turbulence level is unknown, however by adding ten percent of turbulence, $0.01U^2$, a realistic variation of the Nusselt number is captured. It should be noted that the ribs produce a large amount of turbulence that effectively hide any discrepancies made in the inlet specification.

4 RESULTS AND DISCUSSION

The combination of the new wall treatment of Bredberg and Davidson (2002) with the improved $k-\omega$ model of Bredberg et al. (2002) was used to predict the flow field and heat transfer levels

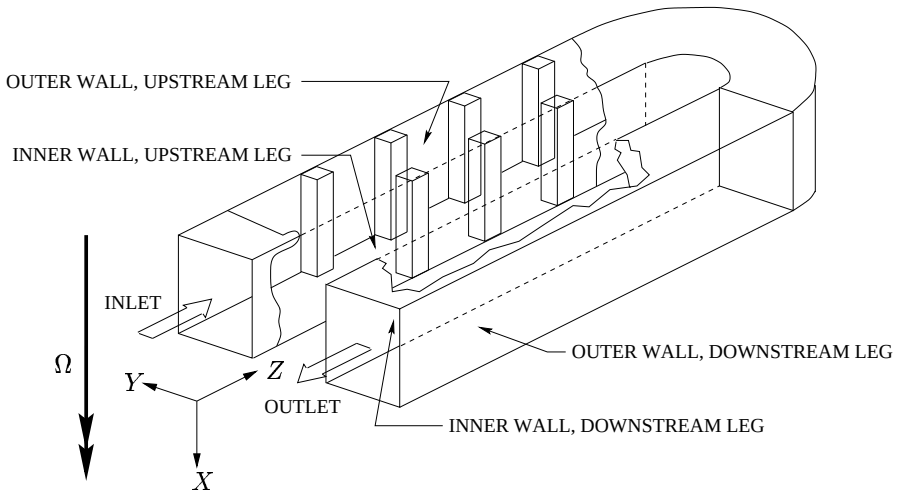

Figure 1: U-duct with rib-roughened walls

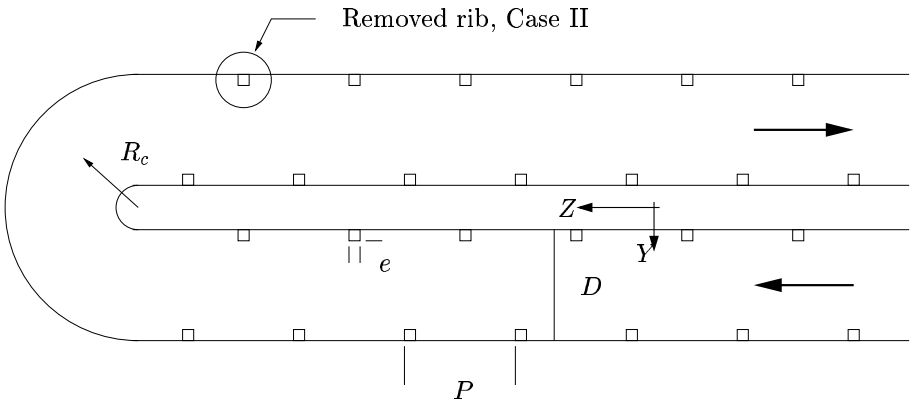

Figure 2: Rib-configuration, Case II and Case III

in a stationary and rotating rib-roughened U-bend, see Figure 1.

The configuration selected here is the same as the one investigated by Iacovides et al. (1998) and Iacovides et al. (1999). The former work measured velocity data at a Reynolds number of 100 000, while in the latter paper, heat transfer data were presented at a slightly lower Reynolds number, $Re_D = 95\,000$. The U-bend is of square cross-section, $D \times D$ with a 180° bend of a mean radius, $R_c/D = 0.65$. The staggered ribs are located only along the outer and inner wall of the two legs of the U. The rib-height-to-duct-diameter ratio, e/D, is 0.1 and a unity pitch-to-duct-diameter ratio, P/D. The resulting blockage accounts to 10% as $P/e = 0.1$. The ribs closest to the bend are at a distance of $0.45D$ from the bend entry and exit respectively, see Figure 2.

Two different rib-configurations were used in the experiments. The difference between Case II and Case III, notation as used in Iacovides et al. (1999), is that in the former case the first rib along the outer wall in the downstream leg is removed, see Figure 2. Velocity data is available for Case III, (both stationary and rotating), and heat transfer data for Case II (only stationary). The rotational number, $Ro = \Omega H/U_b$ is 0.2, with the clockwise direction positive, as indicated by Figure 1.

The computations were made on a relatively coarse mesh, with $y^+ \approx 5$ for the first near wall node. Each rib-interval used $30 \times 60 \times 58$ nodes ($X \times Y \times Z$). The computational domain includes 8.5 rib-intervals in each leg, for a total of 34 ribs. Note that due to the orthogonal rotation mode a symmetry condition could be applied in the YZ-plane. The total amount of nodes, including the

bend, a short inlet and outlet section is $30 \times 60 \times 1074 = 1.93 \cdot 10^6$.

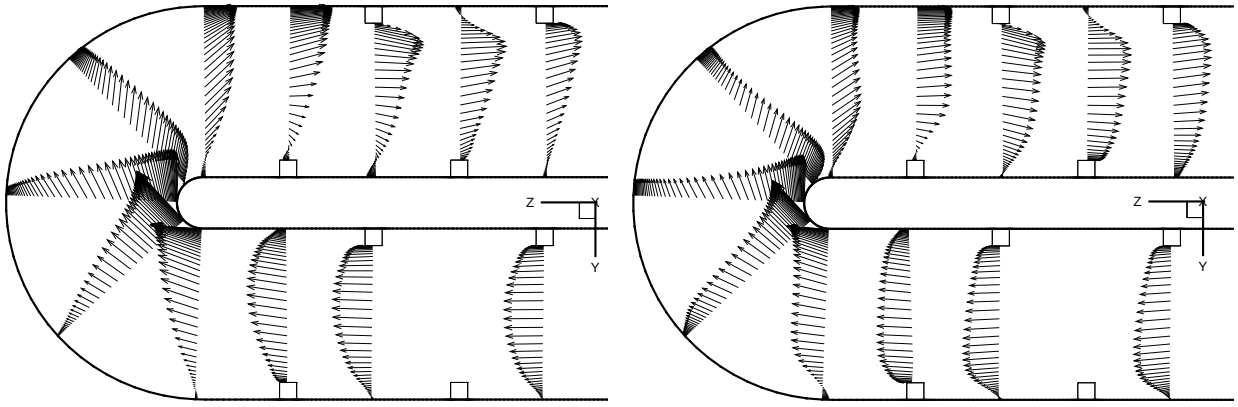

(a) Stationary, $Ro = 0$ (b) Rotating, $Ro = 0.2$

Figure 3: Predicted velocity profiles, symmetry-plane, Case III.

4.1 Flow Field

The predicted velocity-profiles in the symmetry plane for Case III at different locations are shown in Figure 3(a) and Figure 3(b).

After the initial development, the flow behaves in a periodic manner, with repeatedly separations and re-attachments due to the presence of the ribs. Within each rib-interval the main re-circulation bubble stretches for approximately half the rib-interval, see Figure 4(a). The flow stays attached on the channel floor only for a short distance before it separates due to the blocking effect of the next rib. At the upstream corner of the rib, there is also a separation making a small re-circulating zone on the top of the rib. The reader is referred to Bredberg (2002) for a more detail discussion regarding the flow around ribs. These numerous separations produce an increased turbulence level, which is several times higher than that experienced in a smooth channel.

The curvature of the bend produces two contra-rotating vortices which transport fluid from the inner side to the outer side along the symmetry-plane (with a reverse motion along the top wall). In a U-bend of strong curvature, as here, there will be a separation at the inner-wall of the bend, with a consequently strong acceleration along the outer wall at the exit of the bend. This produces a significant amount of turbulence level which increases the heat transfer in the downstream leg, as compared to the upstream leg, see next section. As seen in Figure 3, the upstream influence of the bend is only marginal, however downstream the bend the flow is severely disturbed for several rib-intervals.

System rotation further complicates the flow behaviour with the addition of centrifugal buoyancy and Coriolis forces. Using an incompressible flow solver, as in the present study, the buoyancy effect is neglected. The Coriolis force, being a combination of the rotational speed and flow velocity, significantly alter the flow-field, as can be seen in Figure 3. For a clockwise rotation, the rotational induced secondary flow, similarly to the curvature effect, pushes high-momentum fluid towards the outer wall in the symmetry plane. In the legs this results in a skewed velocity profile as seen in Figure 3(b). Within the bend, there is now an even stronger displacement of fluid towards the outer side, since the rotational and curvature effect act in the same direction.

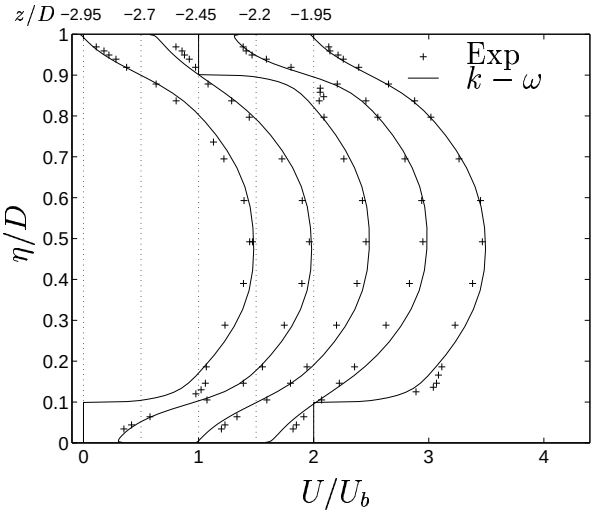

(a) Rib-interval, stationary

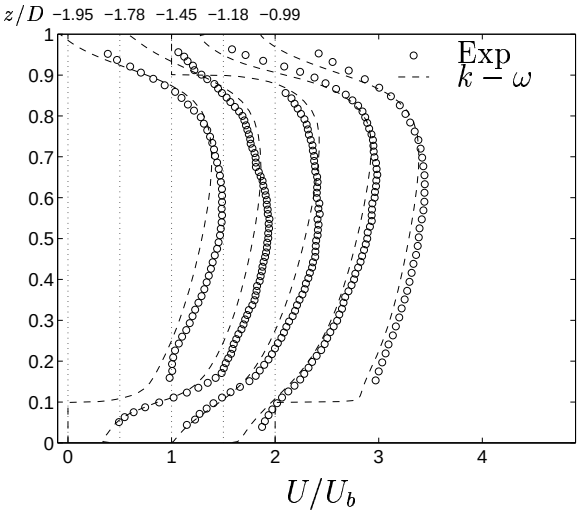

(b) Rib-interval, rotating

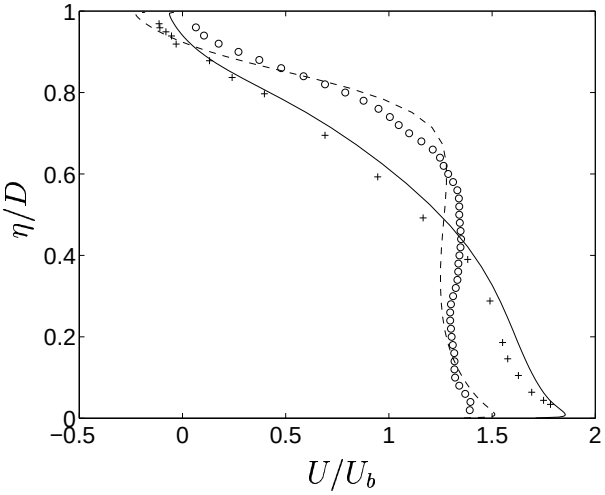

(c) Bend entry, $\theta = 0°$

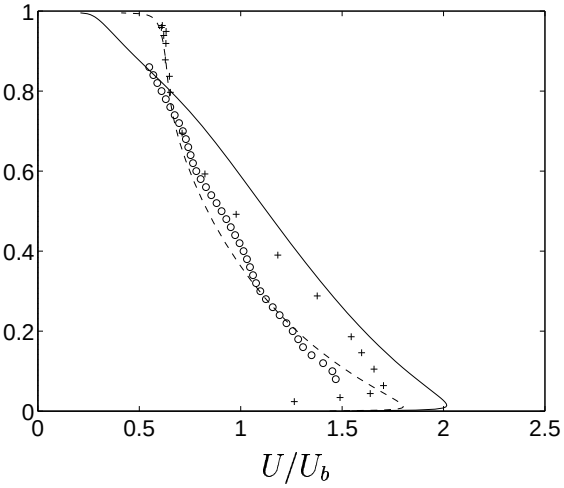

(d) $\theta = 90°$

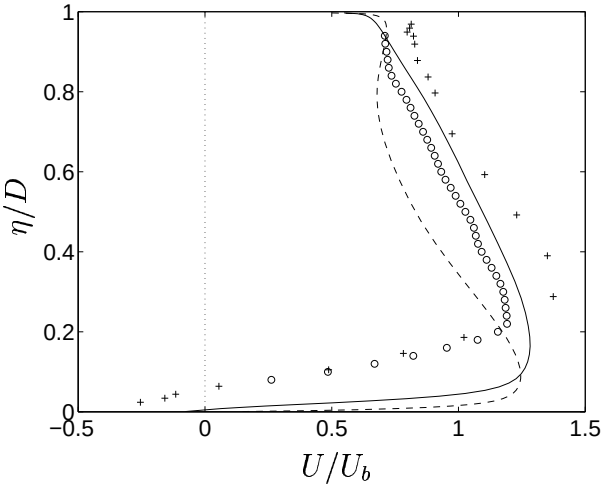

(e) $\theta = 135°$

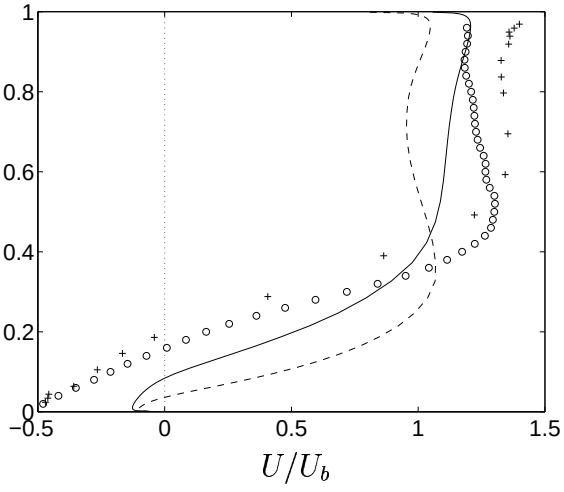

(f) Bend exit, $\theta = 180°$

Figure 4: Profiles of streamwise velocity, symmetry-plane, Case III.

For a counter-clockwise rotation the opposite is true.

A comparison between the predicted and measured streamwise velocity profiles is shown in Figure 4. The details within a rib-interval, Figures 4(a) and 4(b), are taken from the second and first rib-interval upstream of the bend, for the stationary and rotating case, respectively. The centers of the ribs, along the inner wall ($\eta/D = 0$), are located at $z/D = -0.95, z/D = -1.95$ etc. In the stationary case, the agreement is good, apart from in the rib-top region, $0.1 < \eta/D < 0.2$, where the measurement indicates a strong acceleration, which is not captured in the simulations. The re-attachment point is although well predicted midway between the ribs. For rotating conditions, especially along the outer wall there is a larger discrepancy. The proximity of the bend may however corrupt the comparison to the disadvantage of the simulation.

In the bend the agreement between the predicted and measured profiles is less good, which is a consequence of the inability of the two-equation eddy-viscosity turbulence model to accurately reproduce streamline curvature (Iacovides and Launder, 1995). For rotating conditions, an increased separation bubble is predicted in the bend entry, Figure 4(c), while the measurements shows the opposite. Even though the secondary flow is stronger, due to rotation, the measured data does not indicate an increased flow along the outer wall as do the simulations, Figures 4(d) and 4(e). The present simulations are in agreement with those of Iacovides (1999), who used a more advanced second moment closure model. In the measured data the flow separates along the inner wall before $\theta = 135°$ in both the rotating and stationary case while the predicted flow separates closer to the bend exit. At the bend exit, Figure 4(f), predictions and measurements both show that the Coriolis force reduces the flow along the outer side, however the strength of the flow is largely underestimated by the $k - \omega$ model. In addition the simulation is unable to capture the size of the separation bubble along the inner wall.

4.2 Heat Transfer

In the paper by Iacovides et al. (1999) heat transfer measurements were made for Case II under stationary conditions. Figure 5 compares the computed side-averaged Nusselt number in a single rib-interval in the upstream leg. For stationary condition the agreement between the prediction and the measured data is exceptional. There is only a small unphysical fluctuation immediate upstream the rib, at $z/D \approx -2.7$, which is an effect of the coarse mesh. Using a finer mesh, as seen in Figure 6, this anomaly disappears. Unfortunately there are no measured heat transfer data for rotating conditions in the present geometry, however comparing with a similar experiments by e.g. Dutta and Han (1996), indicates a correct trend in the predictions.

It is not possible to make a mesh refinement study on the full rib-roughened U-bend, noting the already large amount of nodes employed. Instead this is performed on simplified geometries. In Figure 6 a comparison is made between the predicted result from the U-bend, and several computations using periodic boundary conditions in the streamwise direction. Using the latter approach, 3D domains of both square, $D \times D$ (identical to the U-bend) and rectangular, $4D(\text{wide}) \times D$, cross-section, as well as two 2D domains were used. Under otherwise identical conditions the predicted Nusselt number deviates by more than 10% between the 2D domain and the U-bend geometry. Thus a 2D configuration may be a too rough approximation for a square cross-section duct.

Figure 7 compares measured and predicted side-averaged Nusselt number along the inner and outer wall of the U-duct. In the figure the inlet is located at $z/D = -10.5$ and the outlet at $z/D = 10.5$. $z/D = 0$ denotes the center of the bend. Under stationary conditions the agreement

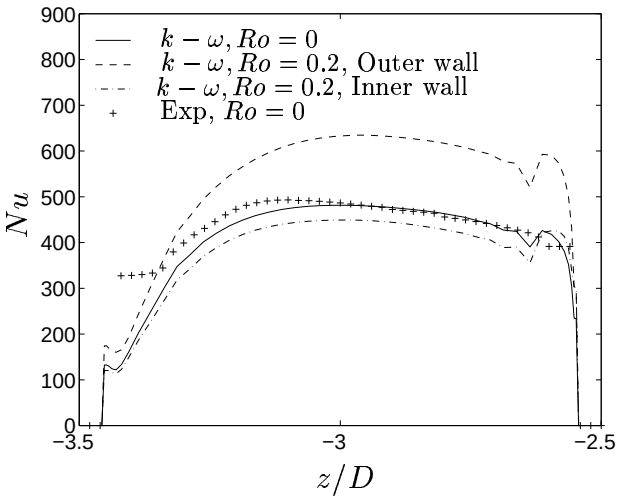

Figure 5: Nusselt number distribution for a single rib-interval. Rotating and stationary conditions, Case II.

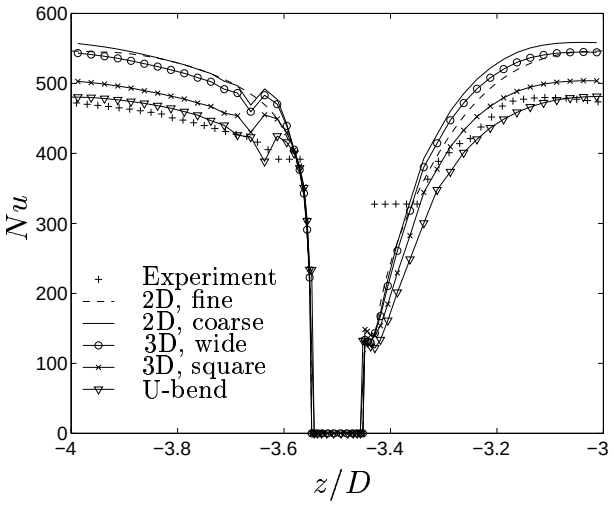

Figure 6: Comparing predicted Nusselt number. 2D, fine: 300×300; 2D, coarse: 58×60; 3D, wide: $58 \times 60 \times 50$; 3D, square: $58 \times 60 \times 30$.

is excellent apart from in the bend-section and immediate after the bend.

Due to lack of measured data, the predicted effect of rotation could only be phenomenologically discussed. Surfaces which are exposed to impinging secondary flows experience a thinning boundary layer, denoted as destabilising conditions. For rotation, as in Figure 1, this condition appears for the outer side, and as a consequence an increased heat transfer level will be predicted, as noted in Figure 7(a). The opposite is true for stable surfaces, i.e. the inner side which will have a thickening boundary layer and hence a reduction in heat transfer, Figure 7(b).

The experiment by Dutta and Han (1996), although at significantly lower Reynolds number of $Re_D = 5\,000$, and with 60° angled ribs ($P/e = 10, e/D = 0.125$) showed an increase in heat transfer level along the outer wall in the upstream leg by as much as 40%, for a rotational number of $Ro = 0.15$. In the downstream leg an even higher (50%) increase was achieved. The reduction along the inner wall was 25% and 20%, for the upstream and downstream leg, respectively. The present simulation gives less amplifications, with an increase from 23% at $z/D = -6$ to 32% at $z/D = -3$, for the outer wall in the upstream leg, and with a reduction of only 6% for the inner wall. In the downstream leg, far from the bend, the amplification is less than 20% for the outer wall. Along the inner wall the reduction is around 10%. It should however be noted that there is a strong influence of both the Reynolds and rotational number on the Nusselt number, and hence the above comparison with the Dutta and Han (1996) experiment could only serve as a guidance.

5 CONCLUSION

In this study calculations were presented for flow and heat transfer in a rotating rib-roughened U-bend. The advantage of using the improved $k-\omega$ turbulence model, Bredberg et al. (2002) with a modified near-wall treatment, Bredberg and Davidson (2002), was documented. With the present mesh, and high Reynolds number, $Re_H = 95\,000$, it was not possible to achieve a solution using any other low-Reynolds number turbulence model. The predicted mean quantities were within measuring error in regions away from the bend. In the bend, however, an eddy-viscosity model is indisputable unable to capture the complex physics found there. Future studies will involve the adoption of the near-wall treatment to non-linear eddy-viscosity models.

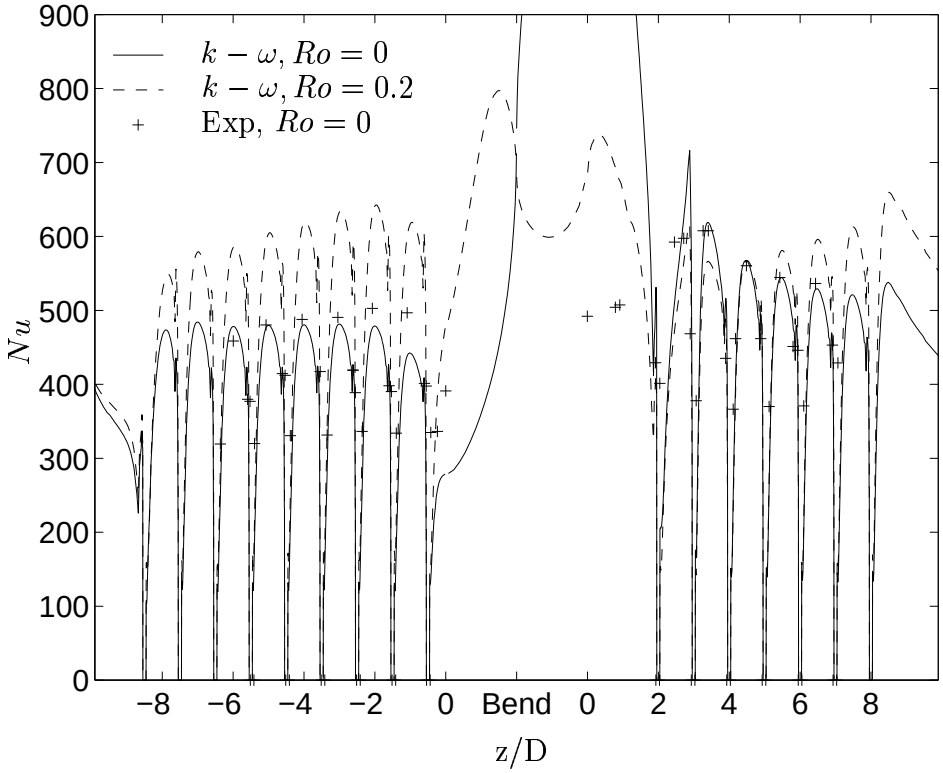

(a) Outer wall

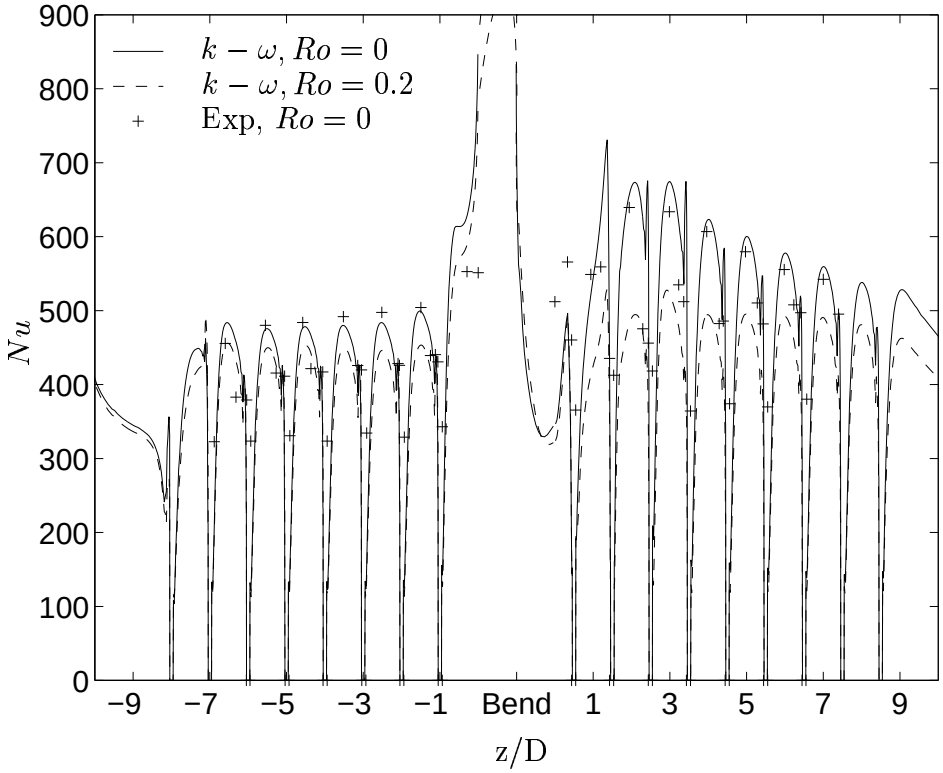

(b) Inner wall

Figure 7: Side-averaged Nusselt number, Case II.

ACKNOWLEDGEMENTS

Funding for the present work has been provided by STEM, Volvo Aero Corporation and ALSTOM Power via the Swedish Gas Turbine Center. The authors gratefully appreciate the help of Dr H. Iacovides for supplying the measurement data.

REFERENCES

Bredberg, J., 2002. Turbulence modelling for internal cooling of gas-turbine blades. Ph.D. thesis, Dept. of Thermo and Fluid Dynamics, Chalmers University of Technology, Gothenburg.

Bredberg, J., Davidson, L., 2002. Low-Reynolds number turbulence models: An approach for reducing mesh sensitivity. Submitted for Journal publication.

Bredberg, J., Peng, S.-H., Davidson, L., 2000. On the wall boundary condition for computing heat transfer with $k-\omega$ models. In: Kim, J. (Ed.), HTD-Vol. 366-5, ASME Heat Transfer Divison - 2000. Vol. 5. The American Society of Mechanical Engineers, Orlando.

Bredberg, J., Peng, S.-H., Davidson, L., 2002. An improved $k-\omega$ turbulence model applied to recirculating flows. Accepted for publication in Int. J. Heat and Fluid Flow.

Craft, T., Gant, S., Iacovides, H., Launder, B., 2001. Development and application of a new wall functions for complex turbulent flows. In: CD-ROM Proceedings of ECCOMAS. Swansea.

Davidson, L., Farhanieh, B., 1995. CALC-BFC. Report 95/11, Dept. of Thermo and Fluid Dynamics, Chalmers University of Technology, Gothenburg.

Dutta, S., Han, J.-C., 1996. Local heat transfer in rotating smooth and ribbed two-pass square channels with three channel orientation. J. Heat Transfer 118, 578–584.

Grotjans, H., Menter, F., 1998. Wall functions for general application CFD codes. In: CD-ROM Proceedings of ECCOMAS. Athens.

Iacovides, H., 1999. The computation of turbulent flow through stationary and rotating U-bend with rib-roughened surfaces. Int. J. Numerical Methods in Fluids 29, 865–876.

Iacovides, H., Jackson, D., Ji, H., Kelemenis, G., Launder, B., Nikas, K., 1998. LDA study of flow development through an orthogonally rotating U-bend of strong curvature and rib-roughened walls. J. Turbomachinery 120, 386–391.

Iacovides, H., Jackson, D., Kelemenis, G., Launder, B., 1999. The measurement of local wall heat transfer is stationary U-ducts of strong curvature, with smooth and rib roughened walls. In: Rodi, W., Laurence, D. (Eds.), 4:th Engineering Turbulence Modelling and Experiments. Elsevier Science Ltd.

Iacovides, H., Launder, B., 1995. Computational fluid dynamics applied to internal gas-turbine blade cooling: a review. Int. J. Heat and Fluid Flow 16, 454–470.

Launder, B., 1984. Numerical computation of convective heat transfer in complex turbulent flows: Time to abandon wall functions? Int. J. Heat and Mass Transfer 27, 1485–1491.

Wilcox, D., 1993a. Comparison of two-equation turbulence models for boundary layers with pressure gradient. AIAA Journal 31, 1414–1421.

Wilcox, D., 1993b. Turbulence Modeling for CFD. DCW Industries, Inc.